Present Status of X-Ray FELs[1]

Kwang-Je Kim and Zhirong Huang

Advanced Photon Source, Argonne National Laboratory, Argonne, IL 60439, USA

Abstract. We review the current status of the theoretical and experimental efforts to develop high-gain free-electron lasers for generating x-ray beams. Such a source will provide ten orders of magnitude brightness enhancement and two orders of magnitude time resolution compared to the current third-generation sources.

I THE PROMISE

The third-generation synchrotron radiation facilities have been highly successful in machine operation and in scientific output. The success derives from the high brightness of the spontaneous emission from undulators in the straight sections of optimized electron storage rings. The brightness (in units of photons per sec per mm^2 per $mrad^2$ per 0.1% relative bandwidth) is about 10^{20} in the wide spectral range from visible to hard x-ray wavelengths. Additional characteristics are the tunability of spectrum and the adjustability of the polarization. The photon beams consist of bunches that are about a few tens of picoseconds long. The bunch length defines the minimum time resolution. The peak brightness during the bunch duration is about 10^{23}.

For the spontaneous radiation discussed above, the radiation intensity is an incoherent sum of contributions from individual electrons. For a high-brightness electron beam passing through a long undulator, the radiation-electron beam system becomes a high-gain free-electron laser (FEL) amplifier [1,2]. If coherent input radiation were available, the high-gain amplifier would be an intense, coherent source. For x-rays, the amplifier configuration is not practical due to the absence of the coherent input source. However, even without the input coherent radiation, intense, quasi-coherent radiation can be produced from amplification of the initial spontaneous radiation when the gain of the system is extremely high. Such a configuration is referred to as self-amplified spontaneous emission (SASE).

SASE in the x-ray region appears to be realizable in view of the recent advance in the production of bright electron beams by means of a photocathode rf gun, bunch

[1)] Work supported by the U. S. Department of Energy, Office of Basic Energy Sciences, under Contract No. W-31-109-ENG-38.

TABLE 1. Peak brightness enhancement from undulator radiation to SASE.

	Undulator	SASE	Enhancement factor
Number of photons	$N_e/137$	$N_{lc}Ne/137$	$N_{lc} \sim 10^6$
Transverse phase space	$(2\pi\epsilon_x)(2\pi\epsilon_y)$	$(\lambda/2)^2$	10^2
Pulse duration	10 ps	100 fs	10^2
Peak brightness	10^{23}	10^{33}	10^{10}

compressors, and a high-energy linear accelerator (linac). The Linac Coherent Light Source (LCLS) is a proposal to use the SLAC linac to produce and use SASE at one Angstrom [3]. The SASE beam in this proposal is about one million times more intense than spontaneous undulator radiation. It is coherent transversely (or diffraction limited), with the transverse phase-space area about one hundred times smaller than the partially coherent undulator radiation. The bunch length, being squeezed by the bunch compressor in the begining of the linac for higher peak current, is about 100 femtoseconds, or two orders of magnitude shorter than that of the third-generation sources. The peak brightness of the x-ray SASE is projected to be about ten orders of magnitude higher than that available from third-generation synchrotron radiation sources, i.e., 10^{33} (in normal units). Table 1 summarizes the brightness enhancement factors. The phenomenal increase in peak brightness and the subpicosecond time resolution would open up exciting scientific applications [4].

To fully utilize the capability of SASE, a "fourth generation" user facility [5] will need to employ a superconducting linear accelerator that is operable at a high repetition rate and can drive a farm of SASE and undulator devices, as shown in Fig. 1. The TESLA FEL proposal is a concrete example of a fourth-generation facility [6].

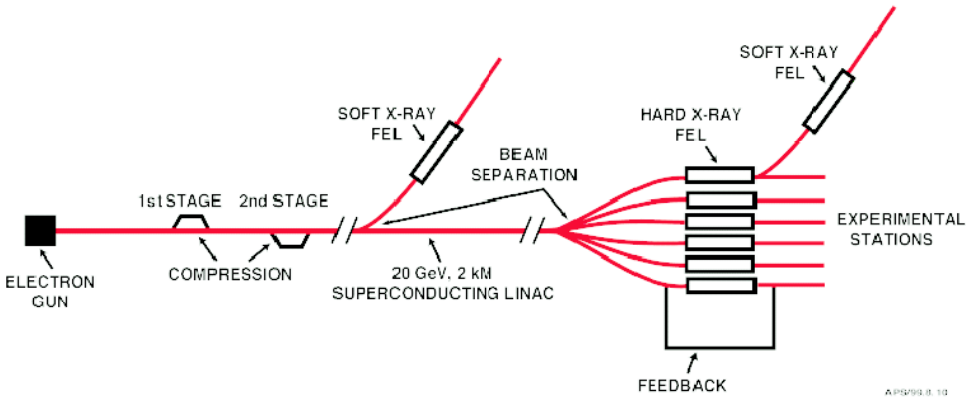

FIGURE 1. Fourth-generation x-ray facility using SASE FELs (from Ref. 5).

II DEVICE REQUIREMENTS

The general components of a linac-based SASE generation are: an rf photocathode gun with emittance corrector, a set of bunch compressors, an acceleration section, and a long undulator.

All accelerators used in experiments to demonstrate SASE take advantage of the low emittance that can be realized with the rf photocathode guns invented at Los Alamos National Laboratory [7] and the emittance compensation scheme [8]. The typical parameters of electron bunches from present rf photocathode guns are: normalized rms emittance $\gamma\epsilon_{x,y}$ of about 5 mm-mrad, bunch charge about 0.5 nC, and pulse length of a few ps. These are adequate for SASE experiments for wavelengths 100 nm or longer. The performance required for a 1-Å SASE, 1 mm-mrad emittance for a 1-nC bunch, appears to be feasible by enhancing various components [9]: optimizing the accelerating gradient and the rf phase, shaping the transverse and longitudinal profiles of the laser pulse, etc.

Although the electron beam from an rf photocathode gun is already bunched to a few picoseconds, it needs to be further compressed to increase the peak current to a few kA to drive an x-ray FEL. In addition to the space charge and the wakefield effect, the bunch compressors must be designed carefully [10] to minimize the emittance dilution effect due to the coherent synchrotron radiation (CSR) [11].

The emittance could also be diluted in the course of the acceleration process in linacs, not only from single particle effects such as focusing mismatch, dispersive effects, and chromatic effects, but also from collective effects due to impedance. Some of these effects, which are due to correlations between different degrees of freedom, can be corrected [10]. Emittance dilution has been extensively studied in connection with linear collider design efforts [12]. Experimentally, it was shown that the increase in the normalized vertical emittance in the SLAC linac, which is about 1.5 mm-mrad in the beginning, can be controlled to less than 50% through the 3-km, 50-GeV acceleration. This is about the level of the control required for the LCLS.

The x-ray SASE requires a long undulator, typically about 100 m long, containing about 1000 periods. The undulator can be divided into several segments with the space between the segments used for diagnostics, focusing, and pumping. The segment must be aligned to an accuracy of a few μm. The tolerance on the magnetic field in each segment is also tight, but within the current state of the art, due to recent developments in undulator construction spurred by the needs of the third-generation synchrotron radiation facilities [13].

III THEORETICAL DEVELOPMENT

The basic theories of high-gain FELs have been well developed in the linear regime [14–17]. Taking into account the effects of beam energy spread, emittance,

radiation diffraction, and optical guiding, the field amplitude at frequency ω can be written as

$$E_\omega(\boldsymbol{x};z) = \sum_n C_n E_n(\boldsymbol{x}) e^{-i\mu_n 2\rho k_u z} + \text{continuum modes.} \tag{1}$$

Here $\boldsymbol{x}$ is the transverse coordinate, z is the distance into the undulator, $k_u = 2\pi/\lambda_u$, λ_u is the undulator period, μ_n and E_n are the discrete and complex solutions for the eigenvalue and the eigenmode of the Maxwell-Klimontovich equations in the frequency domain [18–20], respectively, and C_n is the mode expansion coefficient found by solving the FEL initial value problem [21,22]. The dimensionless parameter ρ is important in determining basic scaling properties of a high-gain FEL [2], and is given by

$$\rho = \left(\frac{eK^2[\mathrm{JJ}]^2 Z_0 j}{32\gamma_0^3 mc^2 k_u^2} \right)^{1/3}, \tag{2}$$

where K is the undulator parameter, [JJ] is the Bessel factor associated with the planar undulator, $Z_0 = 377\ \Omega$, j is the electron current density, and $\gamma_0 mc^2$ is the beam energy. Typically ρ is about 5×10^{-4} for the planned x-ray SASE projects.

A Start-up, Exponential Growth, and Saturation

In the linear regime before saturation, the FEL power spectrum can be expressed as [22]

$$\frac{dP}{d\omega} = g_A \left[\left(\frac{dP}{d\omega} \right)_0 + g_S \frac{\rho\gamma_0 mc^2}{2\pi} \right] \exp\left[\frac{z}{L_G} - \frac{(\Delta\omega)^2}{2\sigma_\omega^2} \right], \tag{3}$$

where $(dP/d\omega)_0$ is the external coherent power spectrum, $L_G = \chi\lambda_u/(4\pi\sqrt{3}\rho)$ is the power gain length, $\chi \geq 1$ is conveniently related to the beam parameters by the interpolating formula given in Ref. [23], and σ_ω is the gain bandwidth. The numerical factors g_A and g_S determine the input coupling to the exponentially growing mode and the effective noise power in units of $\rho\gamma_0 mc^2/(2\pi)$, respectively. It is found that g_A increases from 1/9 to 1 with the increasing initial energy spread for a Gaussian energy distribution [24]. The white noise spectrum, $g_S\rho\gamma_0 mc^2/(2\pi)$, can be interpreted as the coherent fraction of the spontaneous undulator radiation in the first two power gain lengths [25,22]. Thus, g_S increases (from 1) with energy spread and emittance through the increase in gain length. For x-ray SASE FELs, $G = g_A g_S$ can be significantly larger than the one-dimensional, cold beam value (1/9) [21].

As the radiation builds up exponentially after the first two power gain lengths, the phase of most electrons relative to the radiation field changes continuously and eventually the electron beams start to gain energy. At $z = z_{\mathrm{sat}} \approx \lambda_u/\rho \approx 20 L_G$ the

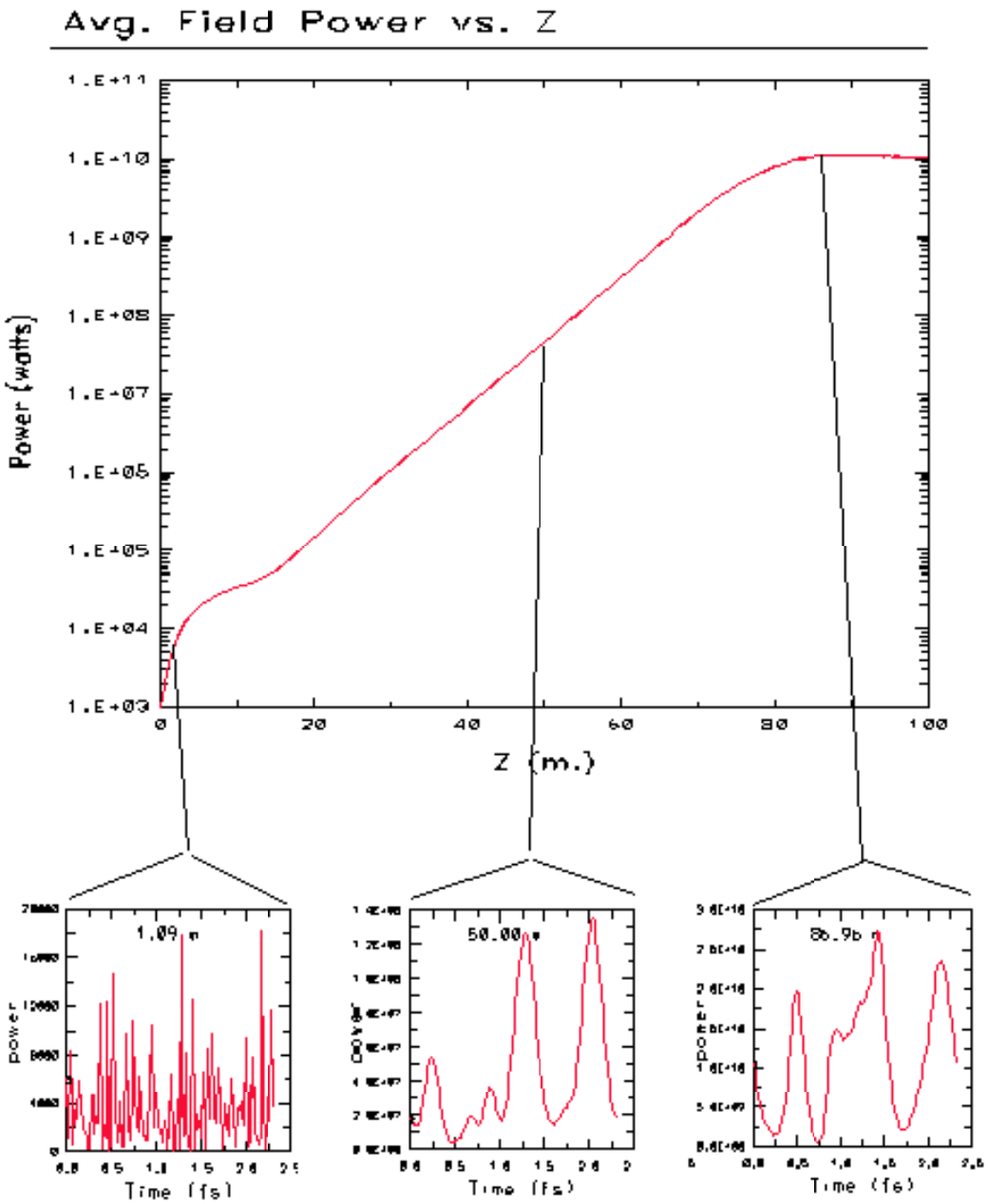

FIGURE 2. Evolution of the LCLS radiation power and the temporal coherence (courtesy of H.-D. Nuhn, SLAC).

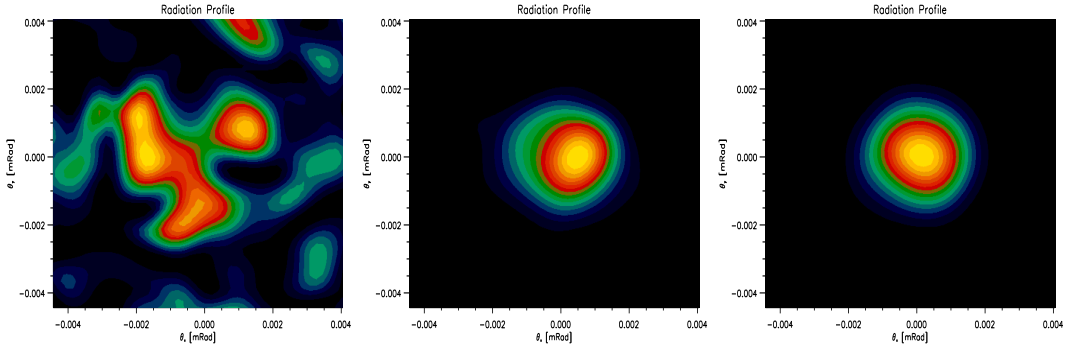

(a) $z = 25$ m (b) $z = 50$ m (c) $z = 75$ m

FIGURE 3. Evolution of the LCLS transverse profiles at different z location (courtesy of S. Reiche, UCLA).

growth of radiation power stops, i.e., *saturates*. A typical power evolution for the LCLS is obtained by GINGER simulation and is shown in Fig. 2. Saturation effects can be studied by a quasilinear extension of the linear theory [16]. The saturated power obtained by this quasilinear approach [26] agrees with an empirical formula obtained through numerical simulations [23], i.e.,

$$P_{\rm sat} \approx \frac{1.6}{\chi^2}\rho P_{\rm beam}, \tag{4}$$

where χ is the gain length degradation factor and $P_{\rm beam}$ is the total electron beam power. After saturation, electrons trapped in the ponderomotive potential of the combined undulator and radiation fields execute synchrotron oscillations, giving rise to the development of sideband frequencies and amplitude modulation of the radiation field [27].

B Transverse Mode Evolution and Coherence

A remarkable feature in the exponential growth regime is optical guiding, the phenomena in which the transverse profile of the radiation beam is frozen. This arises because the field amplitude is dominated by the fundamental mode with the largest growth rate, the imaginary part of μ_1. Higher-order modes usually have a much smaller growth rate and hence are negligible after a few e-folding of the fundamental modes [28]. This process is illustrated in Fig. 3's snapshots of radiation angular patterns at different z locations.

For an axisymmetric electron beam, the fundamental mode of the radiation can be approximated by

$$E_1(\boldsymbol{x}) = \exp\left[-\alpha(\omega)\frac{r^2}{\sigma_x^2}\right], \tag{5}$$

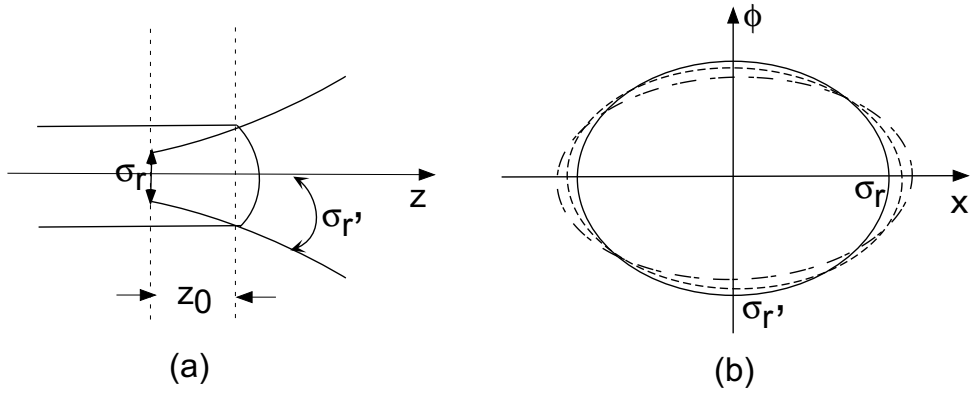

FIGURE 4. Illustration of FEL fundamental mode and the smearing of the transverse coherence.

where $\alpha = \alpha_R + i\alpha_I$ is a complex mode parameter, $r = \sqrt{x^2 + y^2}$, and σ_x is the rms transverse size of the electrons. Such a mode (Fig. 4 (a)) has its minimum waist located

$$z_0 = -\frac{\pi\sigma_x^2}{\lambda}\frac{\alpha_I}{\alpha_R^2 + \alpha_I^2} \tag{6}$$

away from the undulator exit with a Rayleigh length

$$L_R = \frac{\pi\sigma_x^2}{\lambda}\frac{\alpha_R}{\alpha_R^2 + \alpha_I^2}. \tag{7}$$

The rms waist size and the far-field divergence angle are

$$\sigma_r = \sqrt{\frac{\lambda L_R}{4\pi}}, \quad \sigma_{r'} = \sqrt{\frac{\lambda}{4\pi L_R}}. \tag{8}$$

The dominance of a single Gaussian mode means that the SASE FEL at a given frequency is transversely coherent, even though the emittance of the electron beam could be larger than the diffraction limit $\lambda/(4\pi)$. However, taking into account the finite SASE bandwidth, the overall radiation is formed by many fundamental modes with slightly different frequencies and mode parameters; hence the transverse coherence of the overall SASE radiation is somewhat degraded [29]. This degrading effect is illustrated in Fig. 4 (b) as the smearing of the transverse phase ellipses of the radiation beam. Each ellipse, representing a distinct fundamental mode at a particular frequency ω, has almost the same area $\lambda/4$ since the spread $\Delta\lambda/\lambda = \Delta\omega/\omega \sim \rho \ll 1$. However, ellipses are not properly aligned to each other due to the frequency dependence of α in z_0 and L_R. The resulting emittance of the radiation is larger than the minimum emittance $\epsilon_0 = \lambda/(4\pi)$. To quantify the degree of transverse coherence, we introduce a transverse mode number

$$M_T = \left(\frac{\epsilon_r}{\epsilon_0}\right)^2 \tag{9}$$

with the rms emittance of the radiation beam ϵ_r given by

$$\epsilon_r = \sqrt{\langle x^2 \rangle \langle \phi^2 \rangle - \langle x\phi \rangle^2}. \tag{10}$$

Full transverse coherence means that $M_T = 1$. For the LCLS, we find that $M_T \approx 1.06$ before saturation [30], indicating a high degree of transverse coherence for the proposed SASE FEL.

C Temporal Coherence and Intensity Fluctuation

In the exponential growth regime, the spectral bandwidth σ_ω of the SASE radiation decreases as a function of the distance into the undulator as [14,15]

$$\sigma_\omega \approx \omega_0 \sqrt{\frac{\rho}{z/\lambda_u}}, \quad z \leq z_{\rm sat}. \tag{11}$$

At the saturation point $z_{\rm sat} \approx \lambda_u/\rho$ the relative bandwidth becomes $\sigma_\omega/\omega_0 \sim \rho$. Beyond this point, the bandwidth starts to increase due to the development of synchrotron sidebands.

In the time domain the SASE radiation consists of N_e (total number of electrons) wavepackets, each with an rms duration

$$\sigma_\tau = \frac{1}{2\sigma_\omega} \approx \frac{1}{2\omega_0} \sqrt{\frac{z/\lambda_u}{\rho}}. \tag{12}$$

The time domain picture was emphasized by Bonifacio *et al.* [31]. The wavepackets are contained within the bunch length cT of the electron beam, exhibiting M_L coherent regions (spikes). Here the longitudinal mode number

$$M_L \approx \frac{T}{\sigma_\tau} = \frac{T\sigma_\omega}{2} \tag{13}$$

decreases as z increases before saturation (see the inserts of Fig. 2). In general, the pulse length of the radiation field is shorter than that of the electron beam with a smooth current profile because the gain is strongest when the longitudinal current of the electrons is highest. Thus, the number of wavepackets is smaller than given by Eq. (13).

Statistical properties of SASE light are determined by the fact that the field amplitude E_ω is proportional to the sum of a large number of random phase factors. Light with these properties, such as sunlight or spontaneous undulator radiation, is referred to as "chaotic." This topic has been extensively discussed, for example by Goodman [32]. In the context of SASE, it is thoroughly discussed in Ref. [33]. A simple review can be found in Ref. [34]. The probability distribution of the field amplitude E_ω of a chaotic light is Gaussian, as a straightforward application of the

central limit theorem. Equivalently, the intensity at a given frequency $I_\omega = |E_\omega|^2$ has an exponential probability distribution in which the variance is equal to the average intensity. The fluctuation is therefore 100%. In general, we consider a partial flux ΔW as the flux within a 6-D phase-space volume $\Delta\Omega$. The probability distribution of ΔW is given by the "gamma" probability distribution [32]. In the gamma distribution, the fluctuation is reduced by a factor $\sqrt{M}$, where M is the number of coherent modes in $\Delta\Omega$. We can write $M = M_T M_L$, where M_T given in Eq. (9) and M_L given in Eq. (13) are the transverse and longitudinal mode numbers, respectively.

We can now compare the fluctuation in SASE from the LCLS and in undulator radiation from typical third-generation light sources at x-ray wavelengths. For the SASE at saturation, $M_T \approx 1$ (almost full transverse coherence), $\sigma_\omega \approx \rho\omega$, $\rho \approx 10^{-3}$, T is about 100 fs, while for the latter $M_T \approx \epsilon_x\epsilon_y/\epsilon_0^2 \gg 1$, $\sigma_\omega \approx 0.01\omega$, and T is about 100 ps. Therefore the fluctuation in SASE is larger by at least two orders of magnitude than that in undulator radiation.

For most of the SASE demonstration experiments discussed in Section V, the electron bunch lengths with respect to the coherence length are relatively short so that the fundamental SASE fluctuations are large and readily measurable. The fluctuation measurement is therefore a useful diagnostic tool in such cases. For the case of the planned x-ray FEL, however, the overall fluctuation is dominated by the fluctuations from accelerator jitter because the fluctuation from the fundamental SASE property is relatively small.

D Induced Harmonics

When an electron beam is strongly bunched in the ponderomotive potential formed by the undulator magnetic field and the fundamental radiation field, substantial higher-harmonic bunching is induced. Thus, FELs that employ planar undulators are capable of generating intense, coherent harmonic radiation, especially at odd harmonic frequencies.

These induced harmonics have been studied in the context of high-gain FELs using a 1-D model [35] and the 3-D simulation code MEDUSA [36]. Recently, a 3-D theory of harmonic generation has been developed [37], using the coupled Maxwell-Klimontovich equations, that includes electron energy spread and emittance, the radiation diffraction and optical guiding. In general, each harmonic field is a sum of a linear amplification term and a term driven by nonlinear harmonic interactions. After a certain stage of exponential growth, the dominant nonlinear term is determined by interactions of the lower nonlinear harmonics and the fundamental radiation. As a result, the gain length, transverse profile, and temporal structure of the first few harmonics are eventually governed by those of the fundamental. For example, driven by the third power of the radiation field in the fundamental, the third nonlinear harmonic grows three times faster, has an equally coherent transverse mode (with a smaller spot size), and has a more spiky temporal struc-

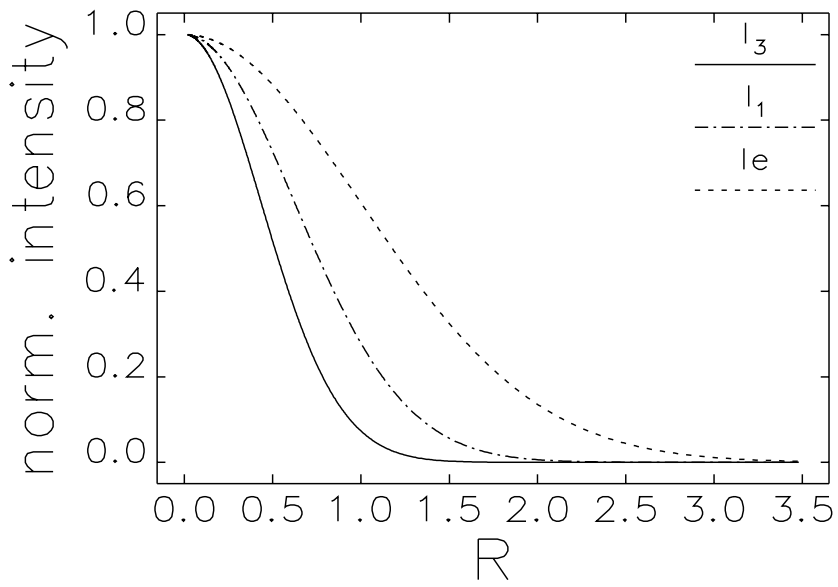

FIGURE 5. Transverse profiles of the LCLS third harmonic (I_3), the fundamental radiation (I_1), and the electron beam (I_e) as functions of the radius R in units of electron beam size.

ture than the fundamental of SASE FELs. For LCLS, the transverse profiles of the third nonlinear harmonic and the fundamental radiation are calculated numerically in the exponential growth regime (see Fig. 5). The evolution of the third-harmonic power is given by [37]

$$\frac{P_3}{\rho P_{\rm beam}} = 0.11 \left(\frac{P_1}{\rho P_{\rm beam}} \right)^3 . \tag{14}$$

Taking $P_1 = P_{\rm sat}/2 \approx 4$ GW before the FEL saturation, one can estimate the third-harmonic power to be 15 MW, about 0.4% of the fundamental power level.

The nonlinear harmonic generation occurs naturally in one long undulator for a SASE FEL and a seeded FEL. As long as the laser fundamental saturates after a certain length of undulator, the induced harmonics are generated around certain levels, much less sensitive to the e-beam parameters, undulator errors, and wake-field effects than other (linear) harmonic generation schemes. The most significant nonlinear harmonic generation is the third-harmonic radiation, typically around one percent of the fundamental power level near saturation. Even harmonics are also present due to the transverse gradient of the beam current. They normally have much lower power levels than their odd counterparts [36,37]. Finally, such a harmonic generation mechanism may be utilized to reach shorter radiation wavelengths or to relax some stringent requirements on the electron beam quality for x-ray FELs.

E Quantum Effects

There are several quantum corrections to the SASE properties. However, these effects are all negligible in the case of x-ray SASE as discussed below [38,39].

First, the quantum correction to the classical gain formula is small if the recoil energy is small compared to the gain bandwidth, or the photon energy is smaller than the electron energy spread. This condition is well satisfied for the x-ray SASE parameters.

Second, the effective noise signal needs to be modified when more than one electron occupies the quantum mechanical unit cell of volume $\lambda\!\!\!^{-3}_c$, where $\lambda\!\!\!^{-}_c$ is the electron's Compton wavelength. This is far from the case in the x-ray SASE.

Third, after taking the quantum effect into account, the mode number M becomes $M/(1+1/\delta)$, where δ, known as the degeneracy number, is the number of photons per mode. This correction is also negligible in the x-ray SASE, since $\delta \gg 1$.

F Simulation Codes

An important tool in designing and analyzing FEL performance is the use of simulation codes with macroparticle models. Each particle, representing tens of thousands of electrons, follows the equations of motion in the combined undulator and radiation fields. The radiation field generated by thousands of simulation particles is then found by solving the paraxial wave equation. A extensive review of FEL simulation codes is given in Ref. [40]. The cross comparison between codes and with theory are generally in good agreement [41]. A steady state code such as TDA [42] is seeded by a monochromatic external radiation field, and hence no variation is allowed along the electron bunch. This approximation permits simulating the electron beam with one slice that is equal to one radiation wavelength λ, thus reducing the requirements for computer resources. MEDUSA, another steady-state code, is extended to include higher hamonics as well as sidebands beside the fundamental frequency [36]. In "time-dependent" simulation codes such as GINGER [43] and GENESIS [44] (both can be run in the steady-state mode), many electron and photon slices along the bunch longitudinal coordinates are tracked by applying an appropriate slippage condition. The time-dependent simulation allows variations along the bunch and is therefore polychromatic around the resonant frequency. Starting up from shot noise can be handled by loading an appropriate amount of random deviation from the uniform longitudinal distribution of the simulating particles [45]. Figures 2 and 3 are examples of GINGER and GENESIS simulations, respectively. The main difference between GINGER and GENESIS is that GINGER assumes an axisymmetric radiation beam, while the radiation field in GENESIS is fully three dimensional. Simulation algorithms based on the integral solution of the paraxial wave equation have been used for RON [46] and FAST [47] to reduce the computation time and to aid design optimization.

IV SCHEMES TO ENHANCE PERFORMANCE

Self-amplified spontaneous emission is the most straightforward approach to achieve extremely high-brightness x-ray sources. Various schemes have been proposed to improve the performance of the x-ray FELs by employing more sophisticated magnetic and optical configurations. We review some of them here.

A High-Gain Harmonic Generation

Although SASE FELs have excellent transverse modes, poor temporal coherence is a limitation imposed by the shot noise buildup because the coherence length $c\sigma_\tau = c/(2\sigma_\omega)$ is usually much less than the bunch length. Without a proper coherent seed at x-ray wavelengths, a high-gain harmonic-generation (HGHG) FEL resorts to a coherent seed at longer wavelengths. In this scheme [48], a small energy modulation is imposed on the electron beam by interaction with a seed laser in a short undulator (the modulator). The energy modulation is converted to a coherent spatial density modulation as the electron beam traverses a dispersive section. A second undulator (the radiator), tuned to a higher harmonic of the seed frequency, causes the microbunched electron beam to emit coherent radiation at that harmonic frequency, followed by exponential amplification until saturation is achieved. The HGHG output radiation has a single phase determined by the seed laser, and its spectral bandwidth is Fourier transform limited [49].

A crucial condition in HGHG FELs is that the beam energy spread entering the radiator section must be made much less than the FEL parameter ρ, in order for the harmonic bunching at the dispersive section to be effective. A successful demonstration experiment has been carried out at Brookhaven National Laboratory (BNL) [49,50], in which a seed CO_2 laser at a wavelength of 10.6 μm produced a saturated, amplified FEL output at the second-harmonic wavelength, 5.3 μm. The intensity of nonlinear harmonic radiation at 2.65 μm and 1.77 μm were determined relative to that of the 5.3-μm fundamental [50]. Cascading several stages of HGHG FELs have been envisioned in order to reach shorter wavelengths [51].

B Regenerative Amplifier

A regenerative amplifier FEL or RAFEL consists of a high-gain undulator and a narrow-band optical feedback system [52]. A small fraction of the SASE signal amplified from shot noise is monochromatized and back-reflected as the input signal for the subsequent amplifications. If mirrors of reasonable reflectivity exist at a certain wavelength range, the steady-state, temporally coherent signal can be achieved after only a few passes of operation. For example, such a scheme has been proposed at the DESY FEL facility at VUV wavelengths ranging from 60 nm to 200 nm [53].

C Two-Stage SASE FEL

Another novel scheme to improve the temporal coherence is the so called two-stage SASE FEL [54], which consists of two undulators (of the same undulator period and strength) and an x-ray monochromator located between them. The first undulator operates in the linear regime of a SASE FEL. After the exit of the first undulator, the electron is guided through a bypass, and the SASE signal enters the monochromator, which selects a narrow band of radiation. At the entrance of the second undulator the monochromatic x-ray beam is combined with the electron beam and is amplified up to the saturation level. Since the SASE power over a narrow bandwidth at the exit of the first undulator fluctuates 100 percent according to the exponential probability distribution, the length of the second undulator is chosen to exceed the saturation length sufficiently to suppress fluctuation of the final output power level.

D X-ray Pulse Compression

The length of an x-ray SASE pulse cT is normally determined by the electron beam, which is about 100 fs. However, it consists of x-ray wavelets, each about $(\rho)^{-1}$ periods, where the FEL scaling parameter $\rho \sim 10^{-3}$. Therefore, it should be possible to compress the SASE pulse to the coherent length at saturation $(c\tau)_{\rm coh} \approx \lambda/\rho$, which is about 1 fs for 1 Å [55]. The compression is accomplished by introducing an energy slew in the electron beam leading to the frequency chirp (frequency shift per unit length). The maximum chirp that can be imposed without degrading the FEL gain is $\frac{\rho}{\lambda/\rho} = \rho^2/\lambda$. The total correlated energy spread in the beam is $(\Delta\omega/\omega)_{\rm max} = \rho^2 T/\lambda$. The chirped pulse can then be compressed with a grating pair. The minimum pulse length after compression given by phase-space conservation is $(c\tau)_{\rm min} = \lambda/\rho$, which is the same as the coherence length at saturation. The technique for pulse compression has been extensively developed for high-power solid state lasers at visible wavelengths. For the x-ray SASE pulse, a major research project will be to demonstrate that the required optical elements exist.

E Variable Polarization

A crossed undulator configuration was proposed for a high-gain FEL for versatile polarization control [56]. It consists of a long (saturation length) planar undulator, a dispersive section, and a short (a couple of gain lengths) planar undulator oriented perpendicular to the first one. In the first undulator, a radiation component linearly polarized in the x-direction is amplified to saturation. In the second undulator, the x-polarized component propagates freely, while a new component polarized in the y-direction is generated from the bunched beam and reaches the same intensity by coherent spontaneous emission. By adjusting the strength of the dispersive section, the relative phase of the two radiation components can be adjusted to obtain a

TABLE 2. Typical parameters of recent SASE FEL experiments.

Main parameters	UCLA/LANL	LEUTL	TTF	VISA
Beam energy [MeV]	18	217	233	71
Energy spread	0.25%	0.1%	0.15%	0.18%
Peak current [A]	170	150	400	200
Normalized emittance [μm]	4	7.5	6	2
Betatron wavelength [m]	1.2	9	4.5	1.8
Undulator period [cm]	2.05	3.3	2.73	1.8
Undulator parameter	1.04	3.1	1.2	1.2
Effective undulator length [m]	2	21.6	13.5	4
FEL wavelength	12 μm	530 nm	109 nm	0.8 μm

suitable polarization, including the circular polarization, for the total radiation field.

V SURVEY OF PROOF-OF-PRINCIPLE EXPERIMENTS

Until recently, FEL experiments operated in the SASE mode have been in the millimeter wavelength range [57]. Driven by intense R&D efforts towards x-ray FELs, a large number of recent SASE FEL experiments push the lasing wavelengths from infrared to visible and on to ultraviolet. We review some of the most significant SASE experiments with the typical parameters given in Table 2.

In the UCLA/LANL experiment [58], radiation intensity at 12 μm is increased by more than 10^4 when the electron charge is changed by a factor of seven (0.3-2.2 nC). Using the measured beam parameters at 2.2 nC, a power gain of 3×10^5 is deduced. The intensity fluctuations are well described by the gamma function distribution with the M parameter evaluated from experimental data.

In the ongoing APS LEUTL experiment [59], exponential gains at 530 nm and 385 nm are measured along the nine undulator sections. With the measured beam parameters, the fitted gain length, near and far-field mode sizes, and radiation spectrum are found to agree with SASE theories. The LEUTL experiment has extensive electron, radiation beam diagnostics (as shown in Fig. 6), capable of measuring SASE evolution as a function of undulator distance z. The longitudinal microbunching of the electron beam along z is observed using coherent transition radiation [60]. With the operation of a bunch compressor, intensity amplification of more than 10^5 is measured, and saturation at both wavelengths is achieved (see Fig. 7). More data collection and analysis are planned at these wavelengths and at shorter wavelengths such as 120 nm.

In the DESY TTF experiment [61], electron beams accelerated by a superconducting rf linac are used to obtain the shortest FEL wavelengths to date. Initial

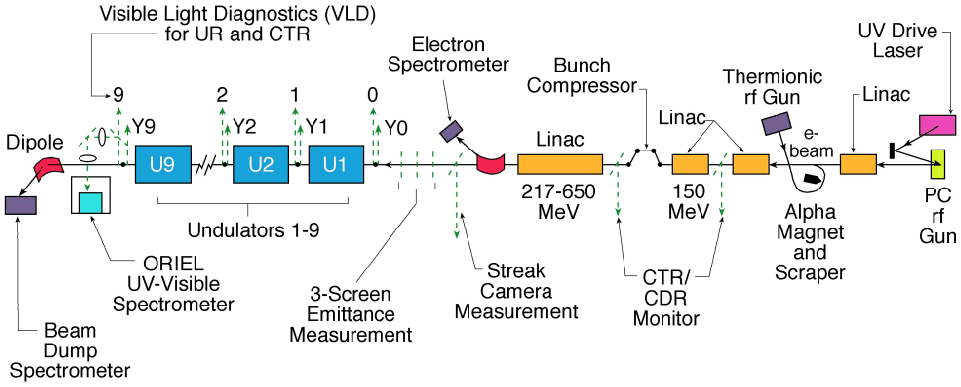

FIGURE 6. Schematic of the electron and radiation beam diagnostics at LEUTL (courtesy of A. Lumpkin, ANL).

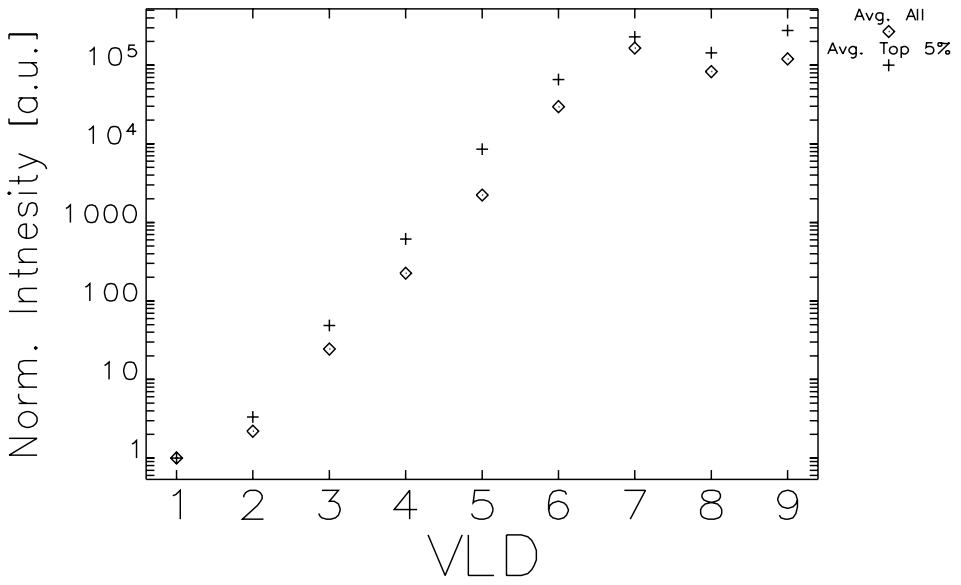

FIGURE 7. Measurements of exponential growth and saturation of 530 nm SASE FEL at LEUTL (each VLD station corresponds to a 2.4-m length of undulator, courtesy of S. Milton, ANL).

results show a gain of about 10^3 from 180 nm to 80 nm, and the radiation characteristics, such as dependency on bunch charge, angular distribution, spectral width, and intensity fluctuation, are all consistent with the present models for SASE FELs.

The VISA group at BNL is commissioning a 0.8-0.6 μm experiment, using a 4-m-long undulator with distributed strong focusing quadrupoles. Initial results show a gain of about 100 [62].

VI CONCLUSIONS

We presented the theoretical advances during the last decade and recent successes in demonstration experiments of high-gain free electron lasers in SASE and other modes of operation for generation of extremely high brightness x-rays. With these developments, the x-ray sciences will have the opportunity to experience another advance as revolutionary as the development of the synchrotron radiation source.

REFERENCES

1. Y.S. Debenev, A.M. Kondratenko, and E.L. Saldin, Nucl. Instrum. Methods Phys. Res. A **193**, 415 (1982).
2. R. Bonifacio, C. Pellegrini and L.M. Narducci, Opt. Commun. **50**, 373 (1984).
3. Linac Coherent Light Source Design Study Report, SLAC-R-521, 1998.
4. LCLS, the first experiments, September 2000.
5. D.E. Moncton, Proceedings of XIX International LINAC Conference, Chicago, IL, USA, 1048 (1998).
6. Conceptual Design of a 500 GeV e+e- Linear Collider with Integrated X-ray Laser Facility, DESY 97-048, 1997.
7. J.S. Fraser, R.L. Sheffield, and E.R. Gray, Nucl. Instrum. Methods Phys. Res. A, **250**, 71 (1986).
8. B.E. Carlsten, Nucl. Instrum. Methods Phys. Res. A, **285**, 313 (1989).
9. D.T. Palmer *et al.*, SPIE **2522**, 514 (1995).
10. P. Emma and R. Brinkmann, Proceedings of the 1997 Particle Accelerator Conference, Vancouver, BC, Canada, 1679 (1997). V.K. Bharadwaj *et al.*, *ibid*, 903 (1997).
11. Ya.S. Derbenev, J. Rossback, E.L. Saldin, and V.D. Shiltsev, DESY Report No. TESLA-FEL-95-05, 1995.
12. T. Raubenheimer, Nucl. Instrum. Methods Phys. Res. A **358**, 40 (1995).
13. E. Gluskin *et al.*, to be published in the Proceedings of the 22^{nd} International Free Electron Laser Conference, Durham, NC, USA, 2000.
14. K.-J. Kim, Nucl. Instrum. Methods Phys. Res. A **250**, 396, (1986).
15. J.-M. Wang and L.-H. Yu, *ibid*, 484 (1986).
16. K.-J. Kim, Phys. Rev. Lett. **57**, 1871 (1986).
17. S. Krinsky and L.-H. Yu, Phys. Rev. A **35**, 3406 (1987).
18. L.-H. Yu, S. Krinsky, and R.L. Gluckstern, Phys. Rev. Lett. **64**, 3011 (1990).
19. Y.H. Chin, K.-J. Kim, and M. Xie, Phys. Rev. A **46**, 6662 (1992).

20. M. Xie, Nucl. Instrum. Methods Phys. Res. A **445**, 59 (2000).
21. M. Xie, presented at the American Physical Society April Meeting, Long Beach, 2000 and to be published in the Proceedings of the 22^{nd} International Free Electron Laser Conference, Durham, NC, USA, 2000.
22. Z. Huang and K.-J. Kim, to be published in the Proceedings of the 22^{nd} International Free Electron Laser Conference, Durham, NC, USA, 2000.
23. M. Xie, Proceedings of the 1995 Particle Accelerator Conference, 183 (1995).
24. E.L. Saldin, E.A. Schneidmiller, and M.V. Yurkov, Nucl. Instrum. Methods Phys. Res. A **313** 555 (1992); see also *The Physics of Free Electron Lasers*, Springer, Berlin, 1999.
25. L.-H. Yu and S. Krinsky, Nucl. Instrum. Methods Phys. Res. A **285**, 119 (1989).
26. N.A. Vinokurov, Z. Huang, O.A. Shevchenko, and K.-J. Kim, to be published in the Proceedings of the 22^{nd} International Free Electron Laser Conference, Durham, NC, USA, 2000.
27. R.W. Warren, J.C. Goldstein, and B.E. Newnam, Nucl. Instrum. Methods Phys. Res. A **250**, 19 (1986).
28. M. Xie, Nucl. Instrum. Methods Phys. Res. A **445**, 67 (2000).
29. E.L. Saldin, E.A. Schneidmiller and M.V. Yurkov, submitted to Opt. Commun., 2000.
30. Z. Huang and K.-J. Kim, to be published.
31. R. Bonifacio *et al.*, Phys. Rev. Lett. **73**, 70 (1994).
32. J.W. Goodman, *Statistical Optics*, John Wiley & Sons, New York, 1985.
33. E.L. Saldin, E.A. Schneidmiller, and M.V. Yurkov, Opt. Commun. **148**, 383, 1998.
34. K.-J. Kim, in *Towards X-ray Free Electron Lasers*, edited by R. Bonifacio and W.A. Barletta, AIP, New York, 1997.
35. R. Bonifacio, L. De Salvo, and P. Pierini, Nucl. Instrum. Methods Phys. Res. A **293**, 627 (1990).
36. H.P. Freund, S.G. Biedron, and S.V. Milton, IEEE J. Quantum Electron. **QE-36**, 275 (2000); Nucl. Instrum. Methods Phys. Res. A **445**, 53 (2000).
37. Z. Huang and K.-J. Kim, Phys. Rev. E **62**, 7259 (2000).
38. K.-J. Kim, in *Quantum Aspects of Beam Physics*, edited by P. Chen, World Scientific, Singapore, 1999.
39. C. Schroeder, C. Pellegrini, and P. Chen, to be published in the Proceedings of the 2^{nd} Workshop on Quantum Aspects of Beam Physics, Capri, Italy, 2000.
40. H.-D. Nuhn, SPIE **3614**, 119 (1999).
41. S. Biedron *et al.*, Nucl. Instrum. Methods Phys. Res. A **445**, 110 (2000).
42. T.-M. Tran and J.S. Wurtele, Computer Physics Comm. **54**, 263 (1989)
43. W.M. Fawley, CBP Tech Note-104, Lawrence Berkeley Laboratory, 1995.
44. S. Reiche, Nucl. Instrum. Methods Phys. Res. A **429**, 243 (1999).
45. C. Penman and B.W.J. McNeil, Opt. Commun. **90** 82 (1992).
46. R.J. Dejus, O.A. Shevchenko, N.V. Vinokurov, Nucl. Instrum. Methods Phys. Res. A **429**, 225 (1999).
47. E.L. Saldin, E.A. Schneidmiller, and M.V. Yurkov, Nucl. Instrum. Methods Phys. Res. A **429**, 225 (1999).
48. L.H. Yu, Phys. Rev. A **44**, 5178 (1991).

49. L.-H. Yu *et al.*, Science, **289**, 932 (2000).
50. A. Doyuran *et al.*, to be published in the Proceedings of the 22^{nd} International Free Electron Laser Conference, Durham, NC, USA, 2000.
51. J. Wu and L.-H. Yu, submitted for publication, 2000.
52. J.C. Goldstein, D.C. Nguyen, and R.L. Sheffield, Nucl. Instrum. Methods Phys. Res. A **393**, 137 (1997).
53. B. Faatz *et al.*, Nucl. Instrum. Methods Phys. Res. A **429**, 424 (1999).
54. J. Feldhaus *et al.*, Opt. Commun. **140**, 341 (1997).
55. C. Pellegrini, Nucl. Instrum. Methods Phys. Res. A **445**, 124 (2000).
56. K.-J. Kim, Nucl. Instrum. Methods Phys. Res. A **445**, 329 (2000).
57. T. Orzechowski *et al.*, Phys. Rev. Lett. 54, 889 (1985); D. Kirkpatrick *et al.*, Nucl. Instrum. Methods Phys. Res. A **285**, 43 (1989).
58. M.J. Hogan *et al.*, Phys. Rev. Lett. **81**, 4867 (1998).
59. S.V. Milton *et al.*, Phys. Rev. Lett. **85**, 988 (2000); N.D. Arnold *et al.*, to be published in the Proceedings of the 22^{nd} International Free Electron Laser Conference, Durham, NC, USA, 2000.
60. A.H. Lumpkin *et al.*, Phys. Rev. Lett. **86**, 79 (2001).
61. J. Andruszkow *et al.*, Phys. Rev. Lett. **85**, 3825 (2000).
62. A. Tremaine *et al.*, to be published in the Proceedings of the 22^{nd} International Free Electron Laser Conference, Durham, NC, USA, 2000.